IJISET - International Journal of Innovative Science, Engineering & Technology, Vol. 3 Issue 6, June 2016
ISSN (Online) 2348 – 7968 | Impact Factor (2015) - 4.332
www.ijiset.com

Study the Annealing Temperature Influence on the Mesoporous Silica Aerogel Properties via Supercritical Drying

Ashraf M. Alattar[1,2], Wesam A. A. Twej[1], Matthew Drexler[2], Faisal M. Alamgir[2]

[1]Physics Department, University of Baghdad, Baghdad, Iraq

[2]School of Material Science and Engineering

Georgia Institute of Technology, Atlanta, GA 3003, USA

* Corresponding author

Abstract

In this work, silica aerogels crack free monoliths of proper properties were simply and successfully prepared through homemade autoclave. We have systematically studied the relationship between the densification temperature of the synthesis environment of silica aerogels on their resulting morphological, optical and electrical properties. SEM and BET measurements were employed as structural probes to ascertain the structural differences. There is a systematic correlation between the annealing temperature and aerogel surface area, porosity, as well as pore size. The implemented autoclave was able to produce aerogel monolith of surface area reach to 998.25 g/m2 and low electric conductivity arrive to $1.17*10^{-4}$(s/m), associated with density of 0.047 g/cm3. The microstructure observed is categorized into three types, namely, open cellular foam (the substance that is formed by trapping pockets of gas in solid), fractal (showing a hierarchical repetition of structural features) and isotropic morphology (at the scale of the visible spectrum). the aerogel properties were remarkably varied. While the influence of annealing temperature the reaction setting has gradually influence on the final aerogel properties, however, it is obviously requested for achieving desirable optically and nano-featured products.

Keywords: Aerogel, BET, Autoclave, transmittance

1.Introduction

Through last decade the development of sol-gel techniques has led to fast progress in the deliberate synthesis of porous materials. Silica alcogel can be processed in a number of ways to yield aerogels; the approach taken in this work to produce the silica aerogel was supercritical drying method (SCD) [1, 2].

. These types of materials are of immense important in different applications like absorption, sensing, catalyst, etc. Silica aerogel become quite popular among all other materials, silica aerogel was produced first in the 1930, In the first half of the century (1931, Kistler) [3]. during last decade the synthesis of aerogel has received significant attention because of possessing a number of exceptional physical properties that attract the attention of researchers. Some investigators have studied the use of different precursors and many have focused on modification of synthesis parameters [4]. Many fascinating properties founds in aerogel, is a nanostructured material and according to their structure aerogel have high specific surface area, very low density, and extremely high porosity. Silica aerogels are materials with unusual properties such as high specific surface area (500–1200m2/g), high porosity (80–99.8%), low density (~0.003 g/cm3), high thermal insulation value (0.005W/mK), ultra-low dielectric constant (k = 1.0–2.0) and low index of refraction (~1.05) [5-8]. Based on these properties many different fields of application of silica aerogel have been reported [9,10]. Thermal treatment one of this parameters that have influence on the structure of aerogel. in this study silica aerogel prepared by used the supercritical drying(SCD) by CO_2, this process give advantage to avoid the capillary stress and associated drying shrinkage. the densification process of silica aerogel at high temperature is the last stage of aerogel processes. In order to interpret the effect of temperature, it is important to study the effect densification of silica aerogel at various temperatures. Using(TEOS) for 1 pH value to measure the pores size, pore volume and surface area also see the transparency of each sample at different temperature. in this work there are four different regions were identified from the characterizations of the samples. regions are exhibited a structure densification of bulk at room temperature, 500 ^{0}C, characterized by densification of bulk in 700^{0}C and at 900 ^{0}C. these regions of temperatures show the optical transparency and structures of aerogels samples will be change during change of temperatures of densification.

Experimental

2.1. Materials

The chemicals are used in the synthesis were, tetraethylorthosilicate (TEOS) with> 99.0% purity), spectroscopic grade ethyl alcohol (200 proof > 99.5% purity, N, N, dimethaylformamide (C_3H_7NO)> 99.0% purity) deionized water catalyzed by ammonium fluoride (> 98.0% purity) all supplied from Sigma Aldrich. Deionized water catalyzed by hydrochloric acid (0.15 M,> 99.0% purity, Amresco).

2.2. Procedure

The Silica gels were prepared via a single-step procedure as following; TEOS, ethanol, water, and hydrochloric acid (volume ratios 2.5:10:2: N) where N was varied to achieve final sol of pH1.Under magnetic stirring the sols were heated at 303 K for 30 min. Then 0.5 ml of C_3H_7NO, was adding as drying control chemical additive (DCCA) and left for further 1 hour under magnetic stirring.

The resulting sol was allowed to gel in 3.2 cm diameter plastic tubes and then aged in the same tubes for 36 h at room temperature. In order to remove any unreacted monomer from the gel network, the gels were washed with pure ethanol in five 24 h steps, using fresh ethanol for each successive step**.**

super critical drying of the gel was conducted in specially designed reactor capable of withstanding high pressures at pressure of 1100- 1215 psi and temperature of 45 ^{0}C for 4 h. during this process its necessary to provide optimum mixing between supercritical CO_2 and the solvent that exist in the pores of gel. With end of $SCCO_2$ drying the densification its last stage and that was made with four different temperatures room temperature, 500 ^{0}C,700^{0}C and 900^{0}C.

Camera photo for the implemented autoclave system as well as aerogel samples that prepared under different pH value are presented in Fig. (1).

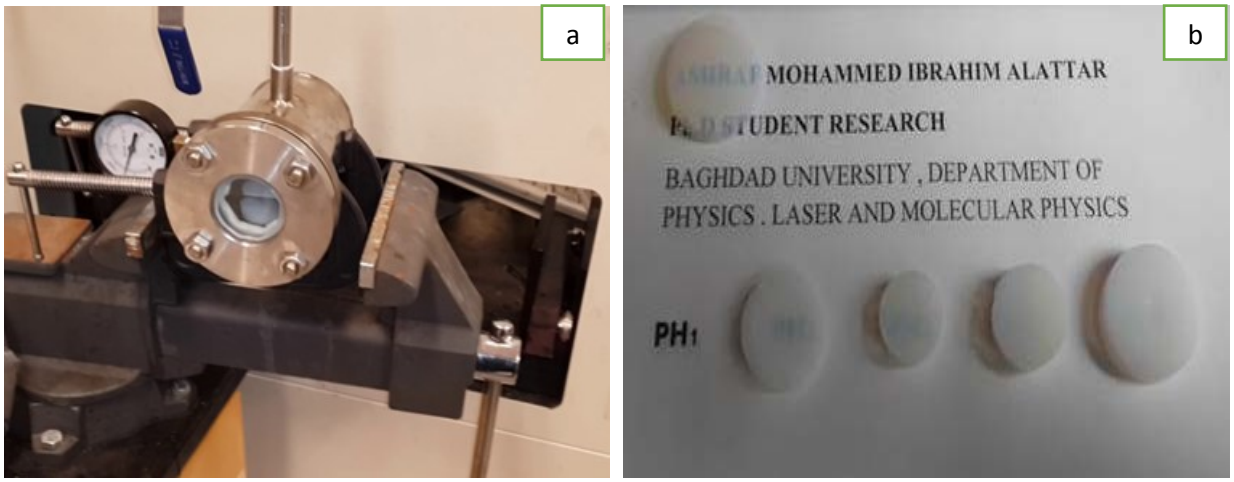

Figure 1: Camera image for (a) Implemented autoclave, (b) some aerogel samples with their preparation pH1 value.

2.3. Characterization of aerogels.

The pore size distribution, pore volume and specific surface area of aerogel samples were determined by Brunauer–Emmitt–Teller (BET) method (micromeritics ASAP 2020).

The morphology and microstructure of silica aerogel samples were observed by scanning electron microscopy (SEM, ULTRA 60) in secondary electron mode.

UV-VIS spectrophotometer (Ultrospec. 4300 pro) was used in this work to record the transmittance of the aerogel samples. FT-IR spectrophotometer (Nicolet Is50) to collects high spectral resolution data for samples of aerogel over spectral range from 400 to 4000 cm^{-1}. A.C conductivity device was used for investigating the behavior of conductivity and dielectric material of disc aerogel. .C measurements, a Hewlett. Packard-R2C unit model (4275 A), multi frequency LCR meter has been used to measure the capacitance (C) and resistance (R) with frequency range between 100Hz-100kHz.

By weighing cylindrical uniform aerogel samples of precise dimensions, the apparent densities were calculated. The dried aerogels were then annealed by heating with different temperature at a rate of 60 °C h^{-1}.

3.RESULTS.

3.1. Surface area and pore size measurements.

various catalyst systems were characterized by BET Nitrogen adsorption-desorption, used to obtain pore volumes and surface areas of the silica aerogel. Utilizing BET analysis method; single condensation point (P/Po = 0.99) was used to find the pore volume and five points, 0.05 <P/Po < 0.35, was conducted to obtain surface areas. The desorption isotherm method was used to calculate pore size distribution. Nitrogen adsorption surface areas were repeated on the same samples and were found to not deviate from the previous measurements more than the expected error of the tests (± 5%), indicating that the small-scale structure does not collapse as a result of capillary pressure from the nitrogen.

The linear isotherm plots for the aerogel samples prepared at several densification temperatures (non-densification ,500 ^{0}C,700 ^{0}C,900 ^{0}C) at final pH 1 value are presented in Figure 2. The influence of annealing temperature on the surface area, pore size, and pore volume are displayed in Figure 2. In general, the surface area of silica aerogels increases as temperature of densification increases, as shown in table1 demonstrate the variation of pore volume and size with final temperature of densification of preparation pH1 value.

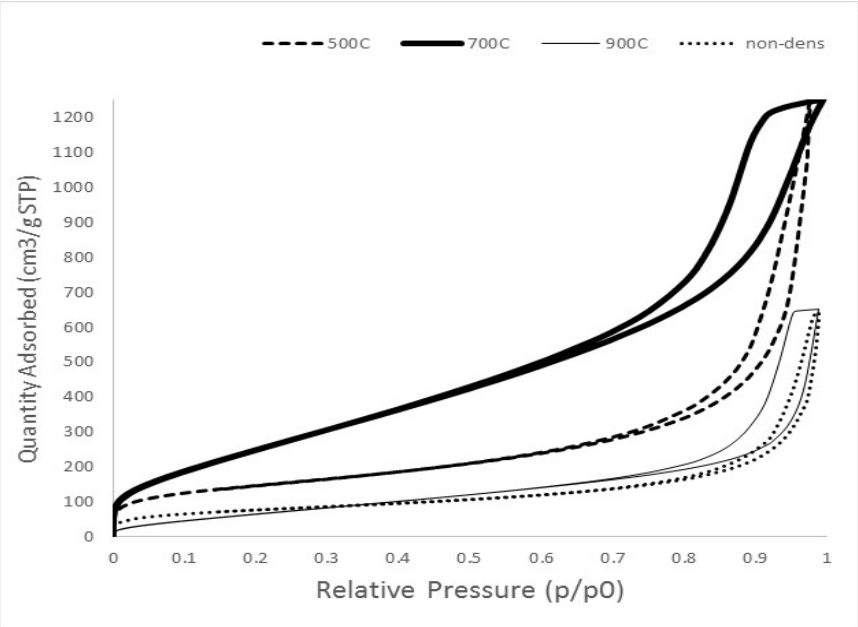

Figure 2: Linear isotherm plot for aerogel prepared at initial pH1 with different temperatures of densification.

the table (1) summarized the nitrogen sorption measurement for the silica aerogel prepared under pH1 value with non-densification and at 500 ^{0}C,700 ^{0}C and 900 ^{0}C of densification temperatures.

Temp (^{0}C)	Surface area (m^2/g)				Pore volume (cm^3/g)			Pore size (Å)		
	BET	Single	BJH ADS	BJH DES	Single	BJH ADS	BJH DES	Single	BJH ADS	BJH DES
Non-dens	279.27	268.24	250.69	257.27	0.58	0.99	1.00	83.13	158.56	156.62
500	531.28	511.95	523.17	557.14	1.62	2.55	2.54	12.19	19.54	18.29
700	998.25	934 .18	1011.09	1105.61	1. 93	1.79	1.82	7.771	7.101	6.593
900	282.75	254 .59	322.83	356.27	1. 01	0.97	0.98	14.272	12.126	11.055

The influence of the densification temperatures of pH1 value on the surface area, pore size and pore volume are Clear through the table 1. The table (1) show demonstrates the variation of pore volume and pore size with final densification temperatures at pH1 value. Without densification yielding maximum pore size and lowest pore volume and surface area, while the densification of aerogel under 700 ^{0}C yielding product of the minimum pore size, pore volume and surface area highest, in other hand the 500 ^{0}C is the moderate between of both.

In other hand, the influence of densification on the densities aerogel bulks summarized in the table 2.

Temp ^{0}C	Mass (gm)	Radius (cm)	High (cm)	Density ρ (g/ cm3)
Non-dens	0.2381	2.7	0.75	**0.055**
500	0.2243	2.7	0.75	**0.052**
700	0.2169	2.7	0.75	**0.050**
900	0.2021	2.7	0.75	**0.047**

Table (2) shows the mass, radius, thickness and density for aerogel bulk samples before and after densification at three different temperatures. Through the step of

densification, it is observed that there are varied differences in the density of these samples regarding to their temperatures of densification.

3.2. Morphology.

Figure 3 show the SEM images of aerogel samples with pH1 value with non-densification and with densification temperatures at 500 ^{0}C,700 ^{0}C and 900 ^{0}C. the images show the samples of aerogel have different network structure related to the densification temperatures. The morphology of these samples are classified into distinct categories. The morphology of the four samples can be grouped into three distinct categories, fractal (M1), isotropic (M2), and open cellular foam (M3).
The non-densification and 500 ^{0}C samples have a very similar microstructure that appears to be fractal in nature. The microstructure at 700 ^{0}C sample shows ultrafine structure at the nanoscale, but is fairly isotropic at the 10 and 300 nm scale. At 900 ^{0}C the microstructure of aerogel sample shows the open cellular foam structure.

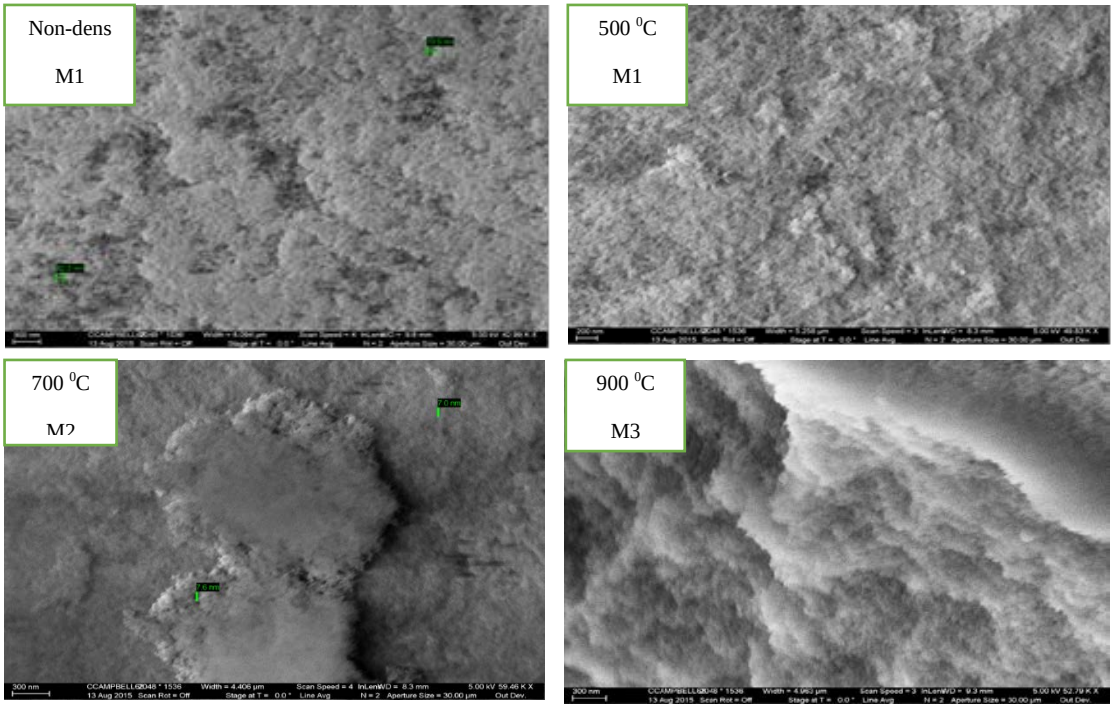

Figure 3: SEM images for aerogel samples prepared with solutions of pH1, at different densification temperatures.

3.3. UV-VIS

Figure 4 presents the transmittance of aerogel samples as function of wavelength at final preparation of pH1 value at different densification temperatures. Interestingly, non-densification and at 900 ^{0}C aerogel samples exhibit minimum transmittance in the entire VIS region, whereas 700 ^{0}C sample show higher transmittance at higher wavelength, and at 500 ^{0}C sample of aerogel have intermediate value.

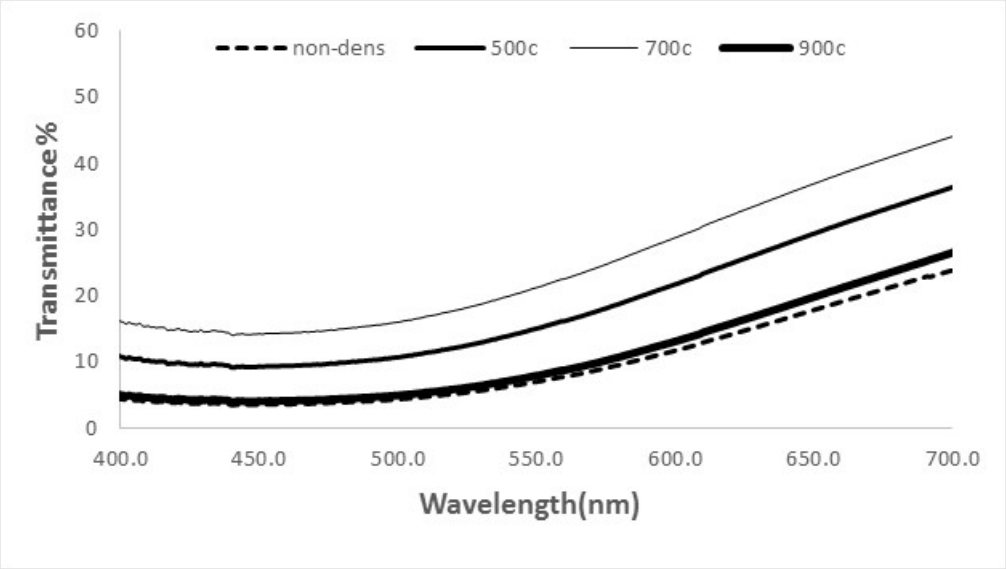

Figure 4: Transmittance spectra for aerogel samples at different densification temperatures.

3.4 FT-IR

The recorded IR transmitted spectra for the prepared aerogel samples are shown in Fig.5. Several absorption bands are marking out in these spectra due to their interesting in our study.

ISSN (Online) 2348 – 7968 | Impact Factor (2015) - 4.332

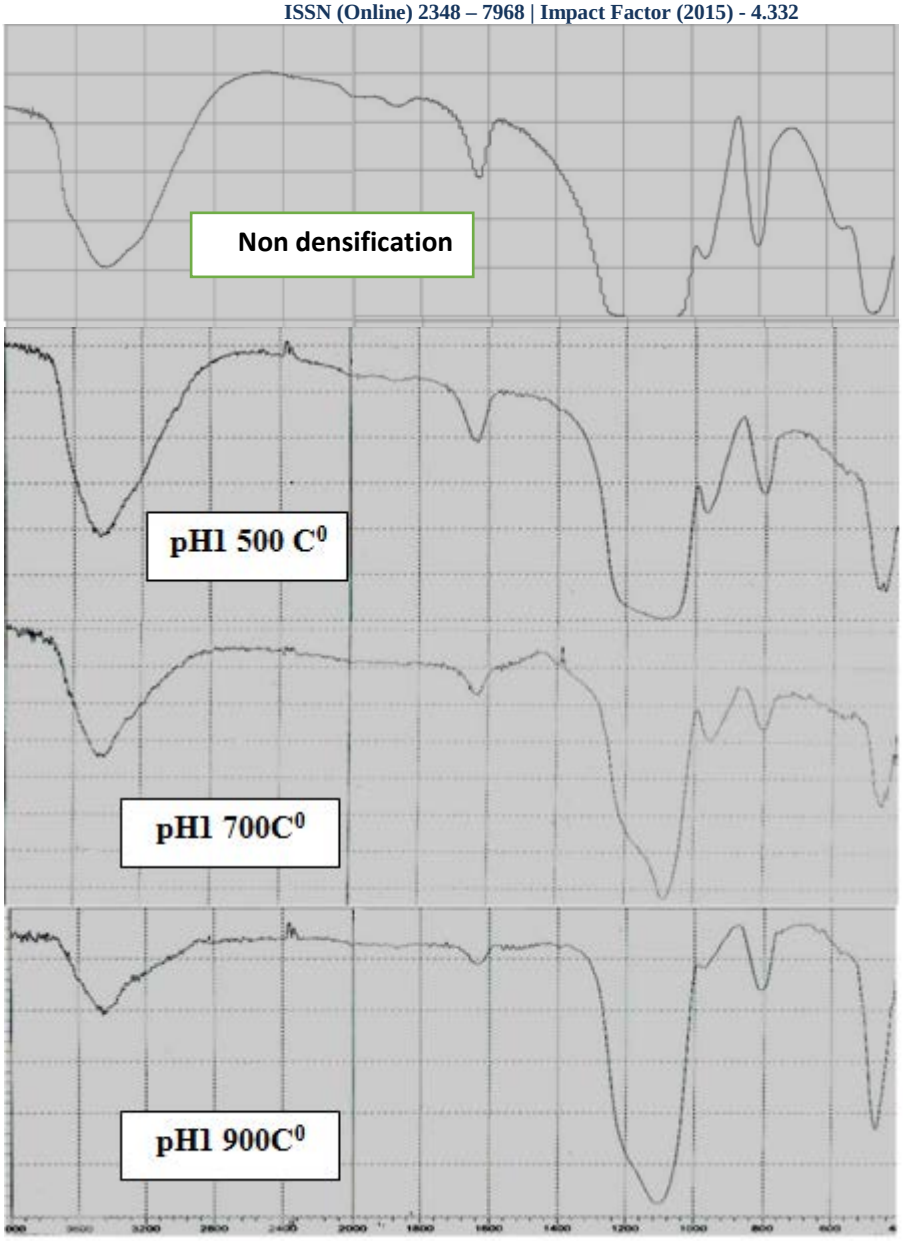

Figure 5: FTIR transmission spectra for aerogel sample pH1 at three different annealing temperatures; 500 °C, 700 °C and 900 °C.

3.5 The A.C conductivity

using thermal evaporation method for layer from aluminium with (0.2) μm thickness on the disc thickness 1 mm for aerogel bulk pH1. The fig.6 show the A.C conductivity $\sigma_{a.c}$ (ω) of silica aerogel sample at different temperatures has been investigated.

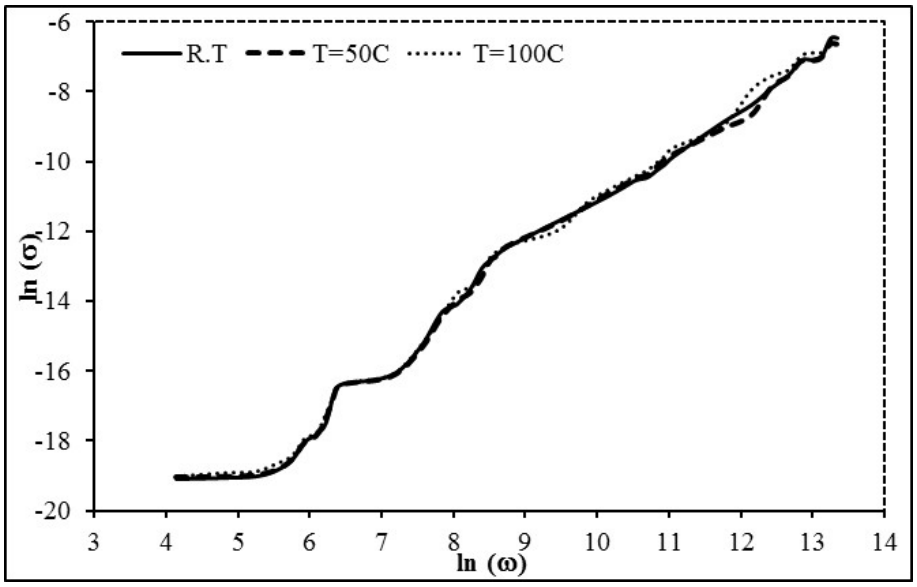

Figure 6: Variation of Ln ($\sigma_{a.c}$) with Ln (ω) at different temperatures.

4. Discussion.

In this work we focus, in our examination, on four samples which can represent without densification and densification at 500 ^{0}C, 700 ^{0}Cand 900 ^{0}C, respectively.

The liner isotherm plots which are presented in Fig. 2 can be examined with the aid of the IUPAC classification hysteresis loops [11]. The plots of samples of pH1, at 700 ^{0}C and 900 ^{0}C in Figure 2 may be classified as H3 type which is related to non-rigid aggregates of plate-like particles (slit-shaped pores). The plots belonging to pH1, without densification and at densification temperature 500 ^{0}C (Figure 2) can be classified as H1 type, related to well-defined cylindrical pore channels [11]. Except in the case of the 500 ^{0}C densification temperature of aerogel sample, the mechanism that produced the linear isotherm plot can be divided into two branches: low densification temperature and high densification temperature behaviour. This may be explained by the fact that silica has its isoelectrical point (IEP), the point at which the zeta potential is equal to zero, at approximately 700 ^{0}C, or 900 ^{0}C, to be exact. At the IEP, the reaction rate for condensation is at a minimum, hence the water condensation mechanism becomes favourable [12]. This condition may give rise to less branchy networks and lead to large pore sizes, resulting in sufficient adsorption quantity at high relative pressure.

The starting pH1 and densification temperature control, therefore, strongly influences the resulting microstructure, and allows for the control of microstructure-dictated properties. Aerogel transmittance spectra in the entire VIS region of pH1at different temperature of densification samples are shown in Fig. (4). It is clear that sample non densification exhibit minimum transmittance whereas pH1 aerogel samples at 500 ^{0}C and 900 ^{0}C show moderated value and at 700 ^{0}C demonstrate the higher transmittance. Highly transparent aerogels are normally prepared using a two-step method [13, 14]. In this work we prepared our samples utilizing a single step method in order to reduce the number of synthesis factors and therefore better establish the influence of annealing on the resulting aerogels.

Subsequently, all samples are made solely of silica, therefore, the aerogel network structure is the individual factor that gives rise to any variation in the transmittance (Figure 4). The difference in refractive index between silica network and the pore material (air in case of aerogel) may be a reasonable source of light scattering, as the pores may act as scatter centres. The transmittance values for the samples at each densification temperature are normalized by the total transmittance for that sample. Since the absorption coefficient of light by silica in the visible region is small, the attenuation of light should result from scattering from the aerogel structure [15]. When the inhomogeneities of the aerogel network are much smaller than the visible wavelengths, nearly isotropic light (Rayleigh) scattering is expected. The resulting microstructure would be M2, from the three canonical structures (M1-M3) identified in Figure 3. The presence of microstructural elements that are on the order of the optical wavelengths, such as those found in the M1 microstructure, can cause Mie scattering. The short-range fractal structures and the strongly localized vibrations of that structure also contribute significantly to scattering the fractal structures scatter significantly as shown in work by Alexander [16]. The maximum of this scattering was shown to occur when the wavelength is close to the size of the fracton. The M1 microstructure from Figure3 typifies this fractal microstructure and is observed in the aerogel samples at 500 ^{0}C and non-densification. The recorded IR transmitted spectra for the prepared aerogel samples are shown in Fig.3. Several absorption bands are marking out in these spectra due to their interesting in our study. Two vibrational bands of silica have appeared in the fingerprint region of the FTIR spectrum, strong centered at around 460 cm^{-1}, and strong and broad at 1104 cm^{-1}that are corresponding to the bending and asymmetric stretching vibrations of (Si—O—Si) groups

respectively, while the symmetric stretching characteristic silica band is weak and has appear at 812 cm^{-1} [17].

Medium and broad O–H vibrations at 3,500 $cm^{-1}$and small sharp at 1,650 cm^{-1}indicate the presence of residual free OH groups (or adsorbed) within the aerogel [18].

FTIR spectra for aerogel samplepH1 at four different annealing temperatures; 500 °C, 700 °C and 900 °Care presented in figure (5) The weak band peak fixed at 965 cm−1 may be ascribed to stretching vibration of silanol (Si—OH) groups [19]. The intensity of this peak was decreasing monotonically with the increase of the annealing temperature. This may be due to the completing of the condensation reaction with temperature yielding more and more conversion of silanol bonds to siloxan bonds (Si—O—Si) [18].

Figure (6) shows the relation between ln(σ)a.c and ln(ω) for silica aerogel at different temperatures. It is clear from the figures that $\sigma_{a.c}(\omega)$ increases with the increasing of the frequency (according to $\sigma_{tot} \sim \omega^{s}$). Hence, it is proposed that two factors are influence σ_t (ω); ions motion and material backbone motion. Furthermore, ions motion is contributed at high frequency [20, 21]. The increasing of σ_t (ω), at low frequencies over (0.01-400) Hz is attributed to the interfacial polarization, since the direct conductivity ($\sigma_{d.c}$) is considerable at this region [22]. The rapidly increasing of $\sigma_t(\omega)$ with increasing frequency at the frequency greater than 10^3 Hz referred to the electronic polarization effect, and the conductivity is pure A. C, conductivity in this region.

Figure (6) also presents the temperature dependence of the A.C. conductivity at different frequencies for aerogel bulk. From this figure (6) can see that there is no distinguish change in the conductivity of the material under study. This may be due to thermal insulation tendency of this material, therefore, it would not allow any transferring of thermal energy as a result of temperature gradient, as a consequence, heat is transferred by phonons (lattice vibration waves) which are unable to vibrate due to thermal energy.

The second part that responsible of heat transfer inside the material is electrons beside the phonons; Figure (6) indicates no effect of this part of thermal conductivity because of the coincidence of these three curves. The outcome from this result is, the material has no free electrons, where the electron contributions is dominant in metals and absent in insulators in thermal conductivity test, hence our material under study

(aerogel) can be considered as an insulating material Whatever the temperature of annealing high.

5. Conclusions.

We demonstrate a systematic correlation between the annealing temperature and the resulting microstructure and optical properties of silica aerogels. Homemade simple designed autoclave can offer aerogel samples of proper physical properties. the temperature densification influence on the aerogel produced yielding highly transparence lower density crackly monolith. at 700 ^{0}C yielding the best surface area, pore size, smaller particle size and pore volume, maximum temperature of annealing give the lowest density through evaporated all the liquid inside the pores with change in the optical and structural properties of aerogel. Therefore, several applications; low densities electrical insulator, optical window, small-pore hydrogen storage tanks etc., could be functionally through adjusting starting catalyst in addition to the annealing temperature as the function of last step to produce the aerogel

Acknowledgements

We would like to acknowledge the National Science Foundation Nanostructured Materials for Energy Storage and Conversion (NESAC) IGERT program for traineeship support under Award Number 1069138. In addition, we thank the Iraqi Ministry of Higher Education and Scientific Research for their generous support.

References

[1] H. Tamon, T. Kitamura, M. Okazaki, J. Colliod Interf. Sci. 19 (1998) 353-359.
[2] A. O. Rami, E. R. Houssam, J. App. Surf.Sci. 257 (2010) 276-281.
[3] S. S. Kistler, Nature 227, 741 (1931).

[4] *A. Soleimani Dorcheh*∗*, M.H. Abbasi*.Silica aerogel; synthesis, properties and characterization njournal of materials processing technology 1 9 9 (2 0 0 8) 10–26.

[5] Kharzheev YN Phys Part Nuclei 39 (2008) 107–135.
[6] Yoldas BE, Annen MJ, Bostaph, Chem. Mater. 12 (8) (2000) 2475–2484.

[7] Carraher Jr., C.E. Polym. News 30 (12) (2005) 386.

[8] Schultz, J.M., Jensen, K.I., Kristiansen, F.H., Sol. Energy Mat. Sol. Cells. 89 (2005) 275.

[9] Jensen KI, Schultz JM, Kristiansen FH JNCS 350 (2004) 351–357.

[10] Bernik DL Recent Pat Nanotechnol 1 (2007) 186–192.

[11] K. S. W. Sing, D. H. Everett, R. A. W. Haul, L. Moscou, R. A. Pierotti, J. Rouquerol, T. Siemieniewska, 57 (4) (1985) 603–619.

[12] C. J. Brinker, R. Sehgal, S. L. Hietala, R. Deshpande, D. M. Smith, D. Lop, C. S. Ashley, Journal of membrane science, 94 (1) (1994) 85-102.

[13] A. Emmerling, R. Petricevic, A. Beck, P. Wang, H. Scheller, J. Fricke, Journal of Non-Crystalline Solids, 185 (3) (1995) 240-248.

[14] T. M. Tillotson, L. W. Hrubesh, Journal of non-crystalline solids, 145 (1-3) (1992) 44-50

[15] K. Athmuri, V. Marinov, Advances in materials science,12 (1) (2012) 5-16.

[16] S. Alexander, Physical Review B, 40 (11) (1989) 7953-7965.

[17] X. Song, N. Jiang, Y. Li, D. Xu, G. Qiu, Chem. Phys. 110 (2008) 128–135.

[18] W. A A Twej, JNCS 382 (2013) 45–51.

[19] W.A.A. Twej, B.T. Chiad, A.J.H. Al-Wattar, F.J. Al-Maliki, IEEE Explor. 3 (2011) 774.

[20] L. Cheng, L. Zheng, G. L. Yao, Q. Y. Jing, J. Nano particles, (2008),1.

[21] C. Zou, J. C. Fothergill, M. Fu, J. K. Nelson, "Improving the dielectric properties of polymers by incorporating nano-particles", Proc. 10th INSUCON International Electrical Insulation Conference, Birmingham, pp. 125-130, 24-26 2006.

[22] G. C. Psarras, E. Manolakaki, G.M. Tsangaris," Dielectric dispersion and ac conductivity in-Iron particles loaded-polymer composites", Composites Part A: Applied Science and Manufacturing, 34(2003)1187-1198.